Available online at www.sciencedirect.com
SCIENCE DIRECT®
Journal of Chromatography A, 1073 (2005) 43–51
JOURNAL OF CHROMATOGRAPHY A
www.elsevier.com/locate/chroma

On the optimisation of the bed porosity and the particle shape of ordered chromatographic separation media

J. De Smet*, P. Gzil, N. Vervoort, H. Verelst, G.V. Baron, G. Desmet

Department of Chemical Engineering, Vrije Universiteit Brussel, Pleinlaan 2, 1050 Brussels, Belgium

Available online 5 November 2004

Abstract

We report on a theoretical study wherein we considered a large number of ordered two-dimensional porous pillar arrays with different pillar shapes and widely varying external porosity and calculated the flow resistance and the band broadening (under retentive conditions) over the complete range of practical velocities using a commercial computational fluid dynamics software package. It is found that the performance of the small porosity systems is very sensitive to the exact pillar shape, whereas this difference gradually disappears with increasing porosity. The obtained separation impedances are very small in comparison to packed bed and monolithic columns and decrease with increasing porosity. If accounting for the current micromachining limitations, a proper selection of the exact shape and porosity even becomes more critical, and different design rules are obtained depending on whether porous or non-porous pillars are considered.

Keywords: Band broadening; Etched columns; Computational fluid dynamics

1. Introduction

The packed bed of spheres, with its fixed particle shape and fixed external bed porosity (around $\varepsilon = 0.4$), has for many decades been the undisputed chromatographic column format. Since the introduction of radically new column manufacturing concepts, cf. the various sol–gel techniques used for the preparation of monolithic packing structures [1–5] and the micromaching techniques Regniers' group [6–8] used to produce their collocated monolithic support structures (COMOSS) column, the bed porosity and the particle shape have become important new design parameters. With appropriate optimization, this additional design freedom could be used to surpass the performance of the currently employed packed bed columns. Due to the increased bed homogeneity, resulting from the fact that the particles are no longer put in place by slurry-packing but are manufactured in situ by means of photolithographic etching techniques, it is especially the COMOSS approach which offers the largest potential increase in performance. Previous calculations by our group have shown that if it would be possible to produce a perfectly ordered array of porous cylindrical pillars with an external porosity of $\varepsilon = 0.4$, reduced plate heights well below unity and separation impedances as small as 200 would come within reach, respectively a factor of 2 and 10 smaller than what is currently achievable with the best possible packed beds [9]. This gain is fully due to the reduction of the *A*-term band broadening. A second potential advantage of the COMOSS concept is to be found in the possibility to move away from the typical $\varepsilon = 0.4$ porosity and round particle shape of the packed bed of spheres. This could open the road towards the achievement of even larger separation resolutions and speeds. There is however, up to now, no real theoretical basis to decide upon the optimal bed porosity and particle shape for such columns. Another problem is that the current generation of COMOSS columns [8,10] are filled with non-porous pillars, leaving the system with a very poor mass loadability and retention capacity. Columns consisting of perfectly ordered arrays of fully porous micro-pillars as discussed and schematically represented in [11] on the other hand would come very close to the ideal chromatographic system, provided they could be manufactured with a sufficient depth and with a sufficient uniformity of the flow-through pore size. Although such porous

* Corresponding author. Tel.: +32 2 6293327; fax: +32 2 6293248.
E-mail address: tw56620@vub.ac.be (J. De Smet).

0021-9673/$ – see front matter © 2004 Elsevier B.V. All rights reserved.
doi:10.1016/j.chroma.2004.10.008

pillar array columns do not exist yet, we hope to contribute to the development of these systems by providing design rules for the optimal bed porosity and particle shape and by pointing at the large potential advantage of such columns.

For this purpose, we have set up a theoretical study wherein we considered a large number of different two-dimensional (2D) porous pillar arrays with varying bed porosity and particle shape and calculated their flow resistance and band broadening (under retentive conditions) over the complete range of practical velocities and characterised them by determining the van Deemter or Knox parameters. These calculations were carried out by means of a commercial computational fluid dynamics (CFD) software package (Fluent, v6.1.22), which has been extended with a number of self-written numerical routines [12,13] to simulate the diffusion and adsorption processes inside the stationary phase.

2. Considered geometries and numerical methods

In the present study, porous pillar array columns with three different pillar shapes (cylinders, ellipsoids and diamonds) and three different external porosities ($\varepsilon = 0.4$, $\varepsilon = 0.6$ and $\varepsilon = 0.8$) have been considered. The lay-out of the different pillar arrays was generated in a commercial CAD program (Gambit v2.1), starting from an equilateral triangular grid and putting a pillar centre on each grid point (Fig. 1). The reader should note that by using the same grid for all particle shapes, the number of trans-channel coupling points remains constant for all pillar shapes. This is important because, as has been pointed out in [6–14], these trans-channel coupling points are needed to overcome the excessive band broadening originating from small pore-to-pore width variations which are inevitable, even when using the best possible currently existing etching processes. We recently confirmed this on a hypothetical segmented column structure [12], showing that even a flow-through pore variability of only a few percent can already lead to a dramatic plate height increase if the number of trans-channel coupling points is too small. Given the difficulties to make any a priori assumptions on the flow-through pore variability of a real, micro-machined porous pillar array column, we therefore think it is critical for any exercise on the determination of the ideal chromatographic packing shape that the number of trans-channel coupling points remains constant. Arrays with a porosity smaller than 0.4 were not considered because such systems yield a dramatic increase of the flow resistance, and arrays with a porosity larger than 0.8 were not considered because such systems would only have a very poor zone ratio $(1 - \varepsilon)/\varepsilon$, leading to poor retention capacities and mass loadabilities.

Apart from the obvious cylindrical pillar shape, we also considered ellipsoidal and diamond-like pillars to investigate the potential advantage of a more elongated and more streamlined shape. For the ellipsoids and the diamonds, the ratio of their maximal lateral (d_{lat}) and longitudinal dimension (d_{ax}) was rather arbitrarily put at $d_{ax}/d_{lat} = \sqrt{3}$. Although other values certainly are possible, the $d_{ax}/d_{lat} = \sqrt{3}$ ratio already gives a significant elongation with respect to the cylindrical pillars, without leading to too locally constricted pore spaces (which is a problem for the ellipsoids in the $\varepsilon = 0.4$ cases [9]), or without leading to a too strong reduction of the fluid contact zone

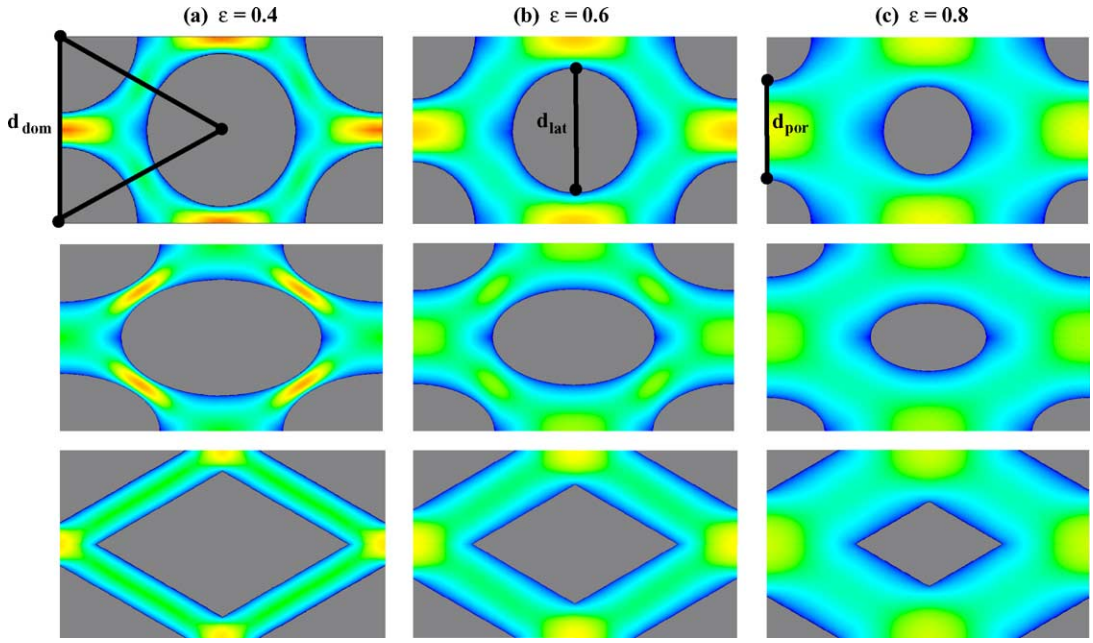

Fig. 1. Overview of the unit cells and the calculated velocity fields for the three different porosities considered pillar shapes: $\varepsilon = 0.4$ (a), $\varepsilon = 0.6$ (b) and $\varepsilon = 0.8$ (c). For each porosity, three different pillar shapes (cylinders, ellipsoids and diamonds) are considered. Represented geometries are for the constant domain size-case.

Table 1
Overview of the most important geometrical and retention parameters of the different considered structures

	d_{dom}	d_{eq}	d_{lat}	d_{por}	τ	k_0''	k'
0.4							
Cylinder	1.23	1.00	1.00	0.23	1.22	0.75	0.714
Ellipsoid	1.23	1.00	0.76	0.13	1.05	0.75	0.714
Diamond	1.23	1.00	0.95	0.24	1.12	0.75	0.714
Plate	1.23	1.00	0.37	0.25	1.00	0.75	0.714
0.6							
Cylinder	1.23	0.82	0.82	0.41	1.16	0.333	1.25
Ellipsoid	1.23	0.82	0.62	0.31	1.11	0.333	1.25
Diamond	1.23	0.82	0.78	0.38	1.10	0.333	1.25
Plate	1.23	0.82	0.25	0.37	1.00	0.333	1.25
0.8							
Cylinder	1.23	0.58	0.58	0.64	1.09	0.125	1.667
Ellipsoid	1.23	0.58	0.44	0.56	1.07	0.125	1.667
Diamond	1.23	0.58	0.55	0.59	1.07	0.125	1.667
Plate	1.23	0.58	0.12	0.49	1.00	0.125	1.667

at the trans-channel coupling points. Fig. 1 also shows that the side of the equilateral triangle forming the basis for the pillar arrangement is the straightforward measure for the domain size (d_{dom}), a measure often used to relate the performance of monolithic silica columns with a different porosity and in the literature on silica monoliths defined as the sum of the pillar size and the size of the flow-through pore neck. In the present study, d_{dom} was nearly always put at $d_{dom} = 1.23$ μm, except for a number of control simulations wherein a 10 times larger domain size was used.

With the above geometrical constraints, the different porosity cases were generated by calculating the diameter (cylindrical pillars) or the lateral width of the pillars needed to obtain the desired volumetric solid zone fraction. The exact geometrical data are listed in Table 1, together with a number of other characteristic parameters. One of these parameters is the equivalent cylinder diameter (d_{eq}), defined as the diameter of the cylinder having the same cross-sectional area A_p as the pillar shape under consideration:

$$d_{eq} = \sqrt{\frac{4}{\pi} A_p} \quad (1)$$

This equivalent cylinder diameter came out a previous constant porosity case study [9] as one of the most suitable characteristic dimensions to bring the van Deemter curves of the different pillar shapes into close agreement.

It should be noted that the presented geometries are for the constant domain size-case. Whereas in this case an increase of the external bed porosity corresponds to a shrinkage of the pillars, the reader should note that in the constant pillar-size case an increasing bed porosity corresponds to an expansion of the through-pore distances and the domain size. The constant particle size case is not represented in Fig. 1, but the reader should bear this difference with the constant domain size case in mind when interpreting the plate height curves in Fig. 2.

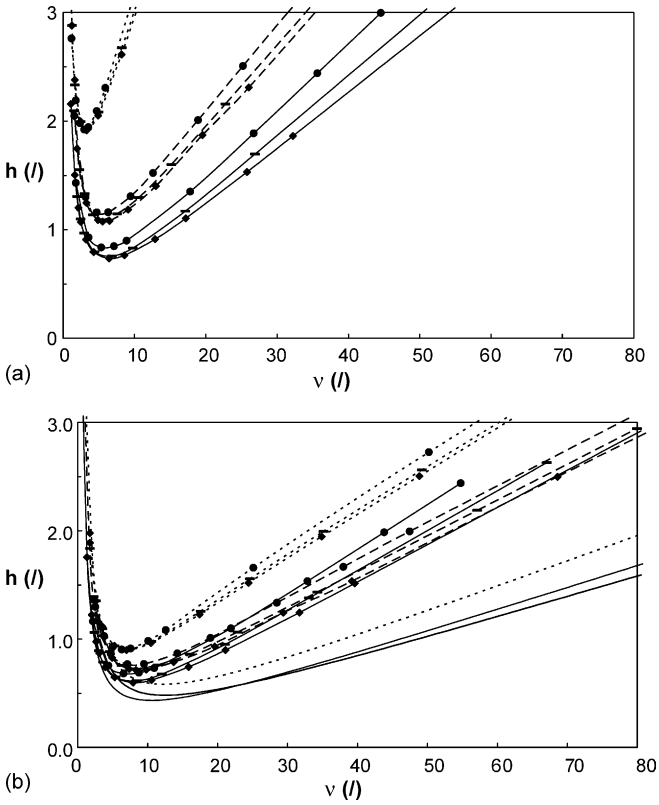

Fig. 2. Reduced van Deemter plots of the band broadening data obtained for the nine different considered porosity (full lines: $\varepsilon = 0.4$, striped lines: $\varepsilon = 0.6$, dotted lines: $\varepsilon = 0.8$) and particle shape ((●) cylinders, (▬) ellipsoids, (♦) diamonds) combinations. The plate height values data were respectively reduced with (a) the equivalent particle diameter (d_{eq}) and (b) the domain size (d_{dom}). The lines without any symbols represent the plate heights determined via Eq. (9) for the parallel plate arrays. See text for further details.

After the generation of a suitable calculation grid (also with the Gambit software), a commercial computational fluid dynamics software package (Fluent, v.6.1) was used to solve the full convection–diffusion material balances across the entire flow domain. The total simulated flow domains consisted of a series connection of 10 unit cells depicted in Fig. 1. So-called velocity-inlet and pressure-outlet conditions were respectively imposed at the front and end plane of the flow domain. Along the sidewalls, a zero normal concentration gradient condition was imposed. With this symmetry condition, the considered flow domain behaves as if it were embedded in an infinitely wide structure. For the same reason, the parts of the sidewalls occupied by the fluid zone were subjected to a slip flow boundary condition (zero normal velocity gradient) to calculate the velocity field. At the surfaces of the porous particles, a no-slip boundary condition ($u = 0$ at the wall surface) was imposed to account for the flow arresting effect of the solid pillar surfaces. Further setting up the problem in the CFD-program, the pillar zones were defined as porous zones with an infinitely large flow resistance. Each individual pillar zone was subsequently also defined as being embedded in a continuous fluid zone, the remaining surface area of the unit cells. As already explained in [13], the software pack-

age was extended with a number of self-written numerical routines to simulate the diffusion and adsorption processes inside the porous pillars. A first user defined function was written to mimic the effect of the slow intra-particle diffusivity. The function was used to attribute the species entering the stationary phase zones a diffusion coefficient different (i.e., smaller) from that in the fluid zone. In all presented cases, the stationary zone diffusion coefficient D_s was always put at 5×10^{-10} m^2/s, whereas the mobile zone diffusion coefficient was always set at $D_m = 1 \times 10^{-9}$ m^2/s. The liquid phase viscosity was always put at $\eta = 10^{-3}$ kg/(m s). A second user defined function was used to subject the species zone to an adsorptive reaction with equilibrium constant K when present in the porous zone. In all simulations, a zone retention factor of $k'' = 2$ was imposed. It should be noted that under this condition, and with the assumption that the internal porosity of the pillars is constant and independent of the external porosity, the different external porosity cases relate to separations with a different phase retention factor k'. The latter can be calculated using:

$$k' = \frac{k'' - k''_0}{1 + k''_0}, \tag{2}$$

with the zone retention factor k''_0 of the unretained species determined by the known external (ε) and internal (ε_{int}) porosities:

$$k''_0 = \frac{1 - \varepsilon}{\varepsilon}\varepsilon_{int} \tag{3}$$

The resulting k''_0 and k'-values are listed in Table 1. The relation between k'', k''_0 and the adsorption equilibrium constant K is given by:

$$k'' = (1 + K)k''_0 \tag{4}$$

The main output of the Fluent simulation program is the concentration versus time response at 10 so-called detection planes, regularly spaced along the flow domain. The recorded break-through curves were subsequently numerically integrated to compute the mean retention time:

$$t_{R,i} = \frac{\int t\,dc}{\int dc} \tag{5}$$

and the variance around this mean:

$$\sigma_i^2 = \frac{\int t^2\,dc}{\int dc} - t_{R,i}^2 \tag{6}$$

With the knowledge of these two measures, the theoretical plate height governing the region between two subsequent detection planes i and j can be calculated using:

$$H = \frac{\sigma_j^2 - \sigma_i^2}{(t_{R,j} - t_{R,i})^2} L_{ij} \tag{7}$$

Apart from the band broadening, the performance limits of a chromatographic system are also determined by the flow resistance. As is a common tradition in chromatography [15], the flow resistance is obtained by plotting the observed pressure drop gradient ($\Delta P/L$) versus the linear velocity (u_0) of the unretained species. From the slope of these lines, it is then straightforward to calculate the resulting column permeabilities (K_v) and flow resistances (ϕ), using:

$$\phi = \frac{d_{ref}^2}{K_v} \quad \text{and} \quad K_v = \frac{u_0 \eta L}{\Delta P} \tag{8}$$

wherein d_{ref} can be any suitable characteristic dimension.

The column permeability in its turn can be used to calculate the column's separation impedance (E), which is a widely used criterium for the efficiency of a column [16].

$$E = \frac{H^2}{K_v} = h^2\phi \tag{9}$$

3. Results and discussion

Fig. 2a shows that, if the systems are compared on the basis of the same equivalent particle diameter, the plate heights depend more strongly on the bed porosity than on the particle shape, i.e., the plate height curves of the different considered geometries are clearly grouped according to their porosity. The influence of the particle shape is the largest in the small porosity case and gradually decreases with increasing porosity, i.e., the difference between the different particle shapes is for example much smaller for the $\varepsilon = 0.8$ case than for the $\varepsilon = 0.4$ case. This can easily be understood from the fact that, with increasing bed porosity, the relative contribution of the mobile zone mass transfer resistance increases over that of the stationary zone mass transfer resistance. This implies that the differences in the C_s-term contribution which exist between the different particle shapes [9] gradually become less important at larger ε and that the main band broadening contribution shifts to the mobile zone. Combining this with the fact that the differences between the flow fields of the different particle shapes are nearly completely vanished in the $\varepsilon = 0.8$ case (Fig. 1c), whereas they are quite significant in the $\varepsilon = 0.4$ case (Fig. 1a), the decreasing influence of the particle shape at large ε becomes quite straightforward.

Comparing Fig. 2a with Fig. 2b, it immediately jumps to the eye that the domain size brings the reduced plate height curves of the different porosity groups much closer to each other than the equivalent particle diameter, although the $\varepsilon = 0.8$ case plate heights still significantly deviate from the $\varepsilon = 0.4$ and the $\varepsilon = 0.6$ cases. Considering a given porosity group, the relative difference between the different particles shapes remains identical to that in Fig. 2a. This can be explained from the fact that the domain size mainly expresses the differences in mass transfer distances between small and large porosity systems and does not contain all information about the microscopic differences of the flow and diffusion geometry. Interpreting both observations in terms of the usefulness of the domain size as a measure to compare the performance of different monolith columns, it should be concluded

that the domain size is a too simple measure to bring plate height curves of different porosity systems into agreement.

On the other hand, cases with a different domain size but with an identical porosity and relative pillar positioning are expected to yield perfectly overlapping h-curves if reduced to the domain size. As outlined by Giddings [17], geometrically similar packings should yield perfectly overlapping (h, ν)-curves if scaled to a characteristic distance allowing to make the structures to perfectly overlap by simply rescaling this characteristic distance. This has been verified by considering cases with a 10 times larger domain size but with an identical porosity and relative pillar positioning. Reducing the obtained plate heights by the domain size, these data also coincide perfectly with the d_{dom}-reduced plate height curves.

As a reference, we also included the performance of theoretical plate heights for an array of parallel plates, theoretically the best performing LC system, but in practice unusable because channel-tot-channel width variations of only 1% limit the system [12,18], for which a well-established analytical solution exists [19,20]:

$$H = \frac{2D_m}{u}\left(1 + k''\frac{D_s}{D_m}\right) + \frac{2}{210}\frac{(1 + 9k'' + 25.5k''^2)}{(1 + k'')^2}\frac{ud_{por}^2}{D_m} + \frac{2}{3}\frac{k''}{(1 + k'')^2}\frac{ud_{lat}^2}{D_s} \quad (10)$$

and which is known to be the system with the smallest possible E-number and plate heights. If comparing the pillar arrays with the parallel plate systems, it should however be kept in mind that the latter does not allow for any trans-channel coupling, and will hence in practice turn out to be too sensitive to small differences in channel width [12]. The values for d_{lat} and d_{por} used in Eq. (10) were respectively calculated as:

$$\frac{2d_{lat}}{d_{dom}} = 1 - \varepsilon \quad \text{and} \quad \frac{2d_{por}}{d_{dom}} = \varepsilon \quad (11)$$

The flow resistance of the plate heights were calculated from the analytical pressure-drop expression for the flow between two parallel flat plates [21]:

$$\Delta p = \frac{12\eta L u_e}{d_{por}^2} \quad (12)$$

Rearranging this expression, and combining it with Eq. (8), the following expression for the u_0-based flow resistance is obtained ($d_{ref} = d_{dom}$):

$$\phi = \frac{48(1 + k_0'')}{\varepsilon^2} \quad (13)$$

Comparing now the parallel plate data with the pillar array plate heights, it can be concluded that a particulate support structure, even though it is perfectly ordered, always yields a significantly larger band broadening as compared to a parallel plate system. The mobile zone mass transfer contribution in a particulate, tortuous bed system is hence significantly different from that in an open-tubular parallel wall flow system. This difference should be attributed to the much more homogeneous longitudinal distribution of the stationary zones in the parallel plate case in comparison to the more point-like distribution of the stationary zones in the pillar array systems, and it is the penalty one has to pay for the presence of flow-through channel coupling points needed to overcome any differences between the flow resistance of adjacent flow channels, which will inevitably be present in any real flow system.

To investigate the relative importance of the mobile and the stationary zone mass transfer resistance, the mobile zone contribution (H_{mob}) has been isolated by subtracting the theoretically known B- and C_s-term contributions from the total plate height, yielding:

$$H_{mob} = H - H_{B_{theo}} - H_{C_{s,theo}} \quad (14)$$

with B_{theo} and $C_{s,theo}$ contributions respectively calculated via Eqs. (15) and (16).

$$H_{B_{theo}} = \frac{B_{theo}}{u_0}D_m \quad \text{with} \quad B_{theo} = 2\frac{1 + \gamma_{sz}k''}{1 + k_0''} \quad \text{and} \quad \gamma_{sz} = \frac{D_{sz}}{D_m} \quad (15)$$

$$H_{C_{s,theo}} = C_s u_0 \frac{d_{lat}^2}{D_m} \quad \text{with} \quad C_s = q\frac{k''(1 + k_0'')}{(1 + k'')^2}\frac{1}{\gamma_{sz}} \quad (16)$$

The shape factor q in Eq. (16) has been determined according to Giddings' original C_s-calculation procedure [17], yielding a value of $q = 1/16.00$ for the cylinders, $q = 1/10.98$ for the ellipsoids and $q = 1/19.28$ for the diamonds. A full account of the calculation procedure is given in [9].

As can be noted from Fig. 3a, the h_{mob}-values which are obtained by reducing H_{mob} with respect to d_{dom} are clearly grouped in three very narrow bundles of curves, one for each value of ε. This implies that the influence of the particle shape is completely eliminated, which can only be explained by assuming that the exact shape of the velocity field only plays a minor role in the total plate height of perfectly ordered pillar array columns. It also implies that the differences between the different particle shapes in Fig. 2 are essentially due to the differences in the C_s-term of the different pillar shapes.

Dividing the h_{mob}-contribution by the total plate height values (Fig. 3b) it can clearly be noted that the relative contribution of the mobile zone mass transfer resistance to the total plate height increases from about 25% for the $\varepsilon = 0.4$ case to over 85% for the $\varepsilon = 0.8$ case. It can hence be concluded that the difference between the different particle shape-induced velocity fields (cf. Fig. 1a) is overshadowed by the much larger difference in stationary zone mass transfer resistance in the case of small ε systems, whereas in the large porosity case, where the mobile zone mass transfer resistance is dominant, the influence of the particle shape upon the velocity field is so small that the difference between the pillar shapes is also nearly completely eliminated.

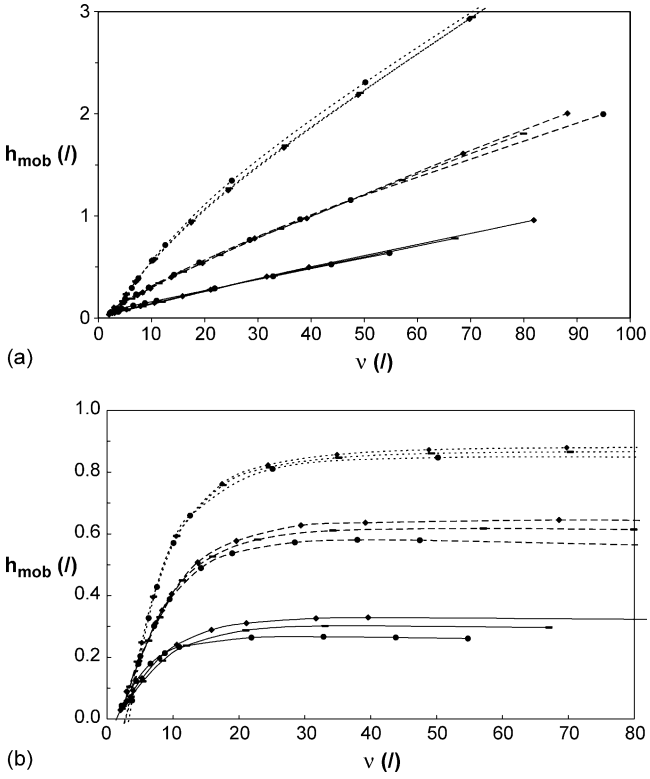

Fig. 3. Variation of mobile phase band broadening contribution (h_{mob}) with ν for the different considered particle shapes (a) and variation of the ratio of h_{mob}/h with ν (b). Same legend key used as in Fig. 2.

Turning now to the flow resistance, the strong decrease of the flow resistance observed when going from the $\varepsilon = 0.4$ case to the $\varepsilon = 0.8$ case (see Table 2) is easy to understand and is in full agreement with previous calculations [22] and with the experimental observations in monolithic columns [23]. Whereas in the small porosity case the flow resistance is a complex function of the bed tortuosity and the pore constriction pattern [9], the flow resistance obviously depends much less on the pillar shape in the large ε case, in agreement with the smaller differences between the different velocity fields.

Chromatographic support systems are very often compared on the basis of their separation impedance, combining both the band broadening and the flow resistance effects [15]. This E-number owes its popularity and usefulness also to the fact that it is independent of the employed geometrical reference basis, and to the fact that it is directly proportional to the absolute minimal analysis time (i.e., if the particle size and the column length are selected such that the column can be operated at its minimal plate height velocity whilst exactly yielding the required number of plates) needed to perform a given separation [15]:

$$t_R = \frac{N^2 \eta}{\Delta p} E_{min}(1 + k') \tag{17}$$

From Eq. (17) and from the E_{min}-values given in Table 1 it can clearly be concluded that the large porosity systems potentially allow for much shorter analysis times than the typical $\varepsilon = 0.4$. For all porosities, the sharper and more longitudinally elongated diamonds perform better than the more round ellipsoidal and circular pillars.

Comparing support performances on the basis of the E-number alone is however not always realistic, as this analysis implicitly assumes that supports with unlimitedly small pillar or domain sizes can be produced. Considering that Eq. (17) is established under the assumption that a system with an optimal equivalent pillar diameter is used, and that this optimal equivalent pillar diameter is given by [15]:

$$d^2_{eq,opt} = \frac{\phi D_m \eta N}{\Delta p} h_{min} \nu_{opt} \tag{18}$$

it can easily be verified, by filling in the appropriate values for the different parameters in Eq. (18), that in many relevant

Table 2
Overview of the chromatographic performance parameters of the different considered pillar shapes

	A[a]	B[a]	C[a]	B_{theo}[b]	C_s[c]	ϕ	h_{min}	E_{min}
0.4								
Cylinder	0.032	2.261	0.042	2.286	0.032	726	0.68	334
Ellipsoid	0.013	2.279	0.038	2.286	0.027	1003	0.61	378
Diamond	0.020	2.252	0.035	2.286	0.024	655	0.60	239
Plate	0.000	2.286	0.021	2.286	0.012	525	0.43	99
0.6								
Cylinder	0.101	2.446	0.033	3.000	0.016	171	0.85	124
Ellipsoid	0.068	2.793	0.033	3.000	0.014	145	0.77	86
Diamond	0.065	2.676	0.032	3.000	0.012	155	0.75	88
Plate	0.000	3.000	0.019	3.000	0.004	178	0.48	41
0.8								
Cylinder	0.204	1.961	0.038	3.556	0.007	53	1.15	71
Ellipsoid	0.197	2.348	0.036	3.556	0.006	43	1.13	55
Diamond	0.180	2.500	0.037	3.556	0.005	48	1.10	57
Plate	0.000	3.556	0.024	3.556	0.001	84	0.58	29

[a] Obtained by fitting Knox' equation (Eq. (18) with $n = 1/3$ and $C = C_s + C_m$) to the h-values shown in Fig. 2b.
[b] Calculated via Eq. (15).
[c] Calculated via Eq. (16).

cases the optimal effective pillar diameter is sub-micron. As an example, it is found for $N = 10{,}000$ and for $\varepsilon = 0.6$ that the optimal diameter for the cylindrical pillars is only 0.26 μm. For $\varepsilon = 0.8$, the optimal pillar diameter is even only 0.20 μm large. It should hence be obvious that such values are impractically small, both from the view-point of mechanical stability as from a pure micro-machining view-point. In order to obtain a competitive mass loadability, porous pillar array columns should preferentially be at least say 10 μm deep, and machining such thin pillar with such a large aspect ratio is currently impossible. It should furthermore also be noted that for an $\varepsilon = 0.6$ array the minimal distance between two pillars is still only roughly one half of the pillar diameter. The distance between the pillars should therefore also be considered as a limiting micromachining factor.

We found it therefore much more practically relevant to consider an optimization exercise wherein the pillar size and the distance between the pillars cannot be made smaller than a given constant. Doing so, so-called Poppe plots [24] are obtained. These plots are obtained by solving the following set of equations as a function of the desired plate number:

$$h = A\nu^n + \frac{B}{\nu} + C_m\nu + C_s\nu, \tag{19}$$

$$t_R = \frac{L}{u_0}(1+k') = \frac{Nd_{ref}^2}{D_m}\frac{h}{\nu}(1+k') \tag{20}$$

$$\nu h = \frac{\Delta p d_{ref}^2}{\phi D_m \eta N} \tag{21}$$

Eqs. (19)–(21) respectively determine the plate height, the analysis time and the pressure-drop in dimensionless coordinates. The pressure-drop limited value of the analysis time is determined as the solution of Eqs. (20) and (21), using Eq. (19) as the link between h and ν. Due to the non-linear nature of Eq. (1), this solution has to be established numerically, except for the cases wherein $n = 0$ or $n = 1$ in Eq. (19). In the present study, different values of n were considered, and the $n = 1/3$ already put forward by Knox and Parcher [25] for the packed bed of spheres turned out to yield the best value. Fittings with other models, like the $n = 1$ exponent coupled Giddings equation (cf. the excellent overview of the different existing plate height equations given in [26]) yielded no significant better fitting. Since most of the A- and C-values cited in literature are for the $n = 1/3$ Knox equation, we also preferred to stick to the latter. The obtained A-, B- and C-values are given in Table 2. It is certainly noteworthy to point at the very small A-term constant values, typically about a factor 5–20 (depending on the porosity) smaller than in real columns, pointing at the extreme reduction of the A-term band broadening which can be expected if it would be possible to produce perfectly homogeneous packings.

As the plate heights in the different porosity systems have been obtained for the same k'' and therefore all have a different k', the plate numbers used in Eqs. (20) and (21) have been corrected by replacing N by N_{eff} on the basis of the $k' = 1.25$-value of the $\varepsilon = 0.6$ case using the following equation.

$$N_{eff} = N\frac{(1+k'_{ref})^2}{k'^2_{ref}}\frac{k'^2}{(1+k')^2} \tag{22}$$

In Eq. (22), $k'_{ref} = 1.25$ and k' and N respectively are the actual phase retention factor for which the given simulation has been carried out (cf. the k'-values given in Table 1) and the obtained plate number for that given k'. Using Eq. (22), it is ensured that the plate heights in Fig. 4 all refer to the same separation resolution R_s.

The Poppe plot given in Fig. 4a is for the case wherein the smallest of the lateral pillar size and the minimal flow-through pore size is put at 1 μm, i.e., it is assumed that the etching tolerances act on both the pillar size and the flow-through pore, and that neither of both can be smaller than 1 μm. For reasons of clarity, the curves for the $\varepsilon = 0.6$ cases have been omitted, and we suffice by saying that they all lied between the $\varepsilon = 0.4$ cases and the $\varepsilon = 0.8$ cases. As can be noted, an $\varepsilon = 0.8$ array with either cylinders or diamonds yields the shortest analysis times and allows to achieve larger maximal plate numbers than the $\varepsilon = 0.4$ arrays. In quantitative terms, it can be concluded that a diamond pillar array with $\varepsilon = 0.8$ yields a six times shorter analysis time than a diamond pillar array with $\varepsilon = 0.4$. The $\varepsilon = 0.8$ array potentially could yield an N_{max} of about 700,000, which is significantly larger than the $N_{max} \cong 200{,}000$ for the $\varepsilon = 0.4$ array. The par-

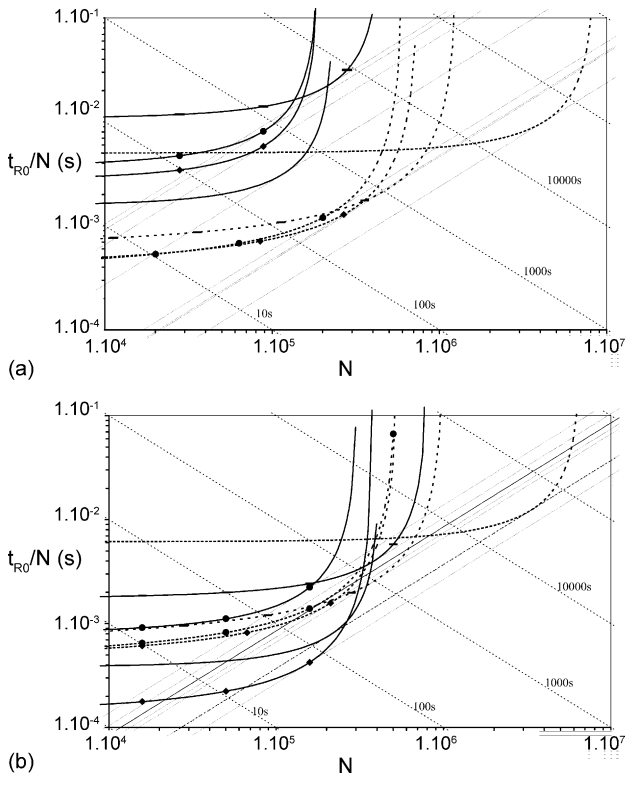

Fig. 4. Poppe plots for the porous pillar (a) and the non-porous (b) pillar cases. The calculated values are for $\Delta P = 200$ bar and for $k'' = 2$ with a minimal limit for d_{lat} and d_{por} of 1 μm. Same legend key used as in Fig. 2.

allel plate array with $\varepsilon = 0.8$ performs strikingly bad in the small N-range, although it has by far the smallest reduced plate heights in Fig. 2b. This poor performance can be explained from the fact that the $\varepsilon = 0.8$ parallel plate case has an extremely large d_{lat}/d_{dom} ratio (cf. Table 1). This implies that if the lateral plate width is put at 1 μm, the corresponding d_{fmin} and d_{dom}-values are significantly larger than in the other cases. As a consequence, the total mass transfer distances in this system are much larger than for the pillar arrays, who all have a significantly smaller d_{lat}/d_{dom} ratio. From the three pillar shapes, the ellipsoidal shape also is the shape with the smallest d_{lat}/d_{dom} ratio, also explaining why the ellipsoidal pillars with $\varepsilon = 0.8$ perform significantly worse than the cylinders and the diamonds. The parallel plate array is obviously only suited in the large N range, although it has to be remarked here that the parallel plate lines should only be considered as purely hypothetical results, because the absence of any trans-channel coupling points makes the parallel plate array extremely sensitive to the polydispersity problem extensively described in [12,18] and most probably limiting the total plate number to $N = 1000$ or even less. It is also interesting to note that the $\varepsilon = 0.4$ arrays are much more sensitive to the exact pillar shape than the $\varepsilon = 0.8$ cases, in full agreement with one's physical expectations.

Since the single current pillar array systems are all non-porous [8,10,14], we also repeated the above design exercise with h-values from which the theoretical C_s-contribution has been subtracted. Since $k_0'' = 0$ for all non-porous systems, all cases now have $k' = k'' = 2$, and the correction in Eq. (22) is no longer necessary. The result is shown in Fig. 4b. The main difference with the porous pillar array cases is that now the $\varepsilon = 0.4$ arrays yield significantly shorter analysis times than the $\varepsilon = 0.8$ arrays. This is of course due to the fact that in the non-porous systems the single relevant mass transfer distance is the pore diameter, in addition to the fact that the most tight machining constraint in the $\varepsilon = 0.4$ cases is on the pore diameter. The $\varepsilon = 0.4$ data in Fig. 4b therefore relate to cases with a pore diameter of $d = 1$ μm. In the $\varepsilon = 0.8$ cases on the other hand, the most tight machining constraint is on the pillar size, such that the $\varepsilon = 0.8$ data on Fig. 4b relate to cases with a lateral pillar size of $d = 1$ μm. Given that in the $\varepsilon = 0.8$ cases the pore diameter is larger than the lateral pillar size, the $\varepsilon = 0.8$ data correspond to systems with a pore size which is significantly larger than the 1 μm value in the $\varepsilon = 0.4$ cases, hence explaining the poorer performance.

4. Conclusions

Due to the assumed perfect homogeneity, the currently considered porous pillar array systems only display a very small A-term band broadening, yielding plate heights and separation impedances which are very small in comparison to the current generation of packed bed and monolithic columns. A proper design of such porous pillar array columns will however be very important, as the performance depends quite strongly on the exact pillar shape (for the small porosity systems) and on the porosity. The present study has also clearly shown that manufacturing constraints can play a major role in the potential performance of porous pillar array systems. If one would be trying to produce such systems, it should be kept in mind that the machining constraints on both the maximal lateral solid size and on the minimal flow-through pore size lead to a situation wherein the most open-porous systems yield the shortest analysis times over the entire range of plate number. For non-porous pillar arrays on the other hand, the small porosity systems are to be preferred over a range of plate heights up to $N = 200{,}000$. In this small porosity case, cylindrical and ellipsoidal pillars perform significantly worse than diamond-like pillars.

Acknowledgements

The authors greatly acknowledge a research grant (FWO KNO 81/00) from the Fund for Scientific Research-Flanders (Belgium). P.G. is supported through a specialization grant from the Instituut voor Wetenschap en Technologie (IWT) of the Flanders Region (grant no. SB/11419). The authors also gratefully acknowledge stimulating discussions with Peter Schoenmakers and Bas Eeltink from the University of Amsterdam (The Netherlands).

References

[1] S. Hjertén, L.J. Liao, R.J. Zhang, J. Chromatogr. 473 (1989) 273.
[2] L.J. Liao, S. Hjerten, J. Chromatogr. 457 (1988) 165.
[3] F. Svec, J.M. Frechet, Anal. Chem. 64 (1992) 820.
[4] H. Minakuchi, N. Ishizuka, K. Nakanishi, N. Soga, N. Tanaka, J. Chromatogr. A 828 (1998) 83.
[5] H. Minakuchi, K. Nakanishi, N. Soga, N. Ishizuka, N. Tanaka, J. Chromatogr. A 797 (1998) 121.
[6] B. He, F. Regnier, J. Pharm. Biomed. Anal. 17 (1998) 925.
[7] F.E. Regnier, J. High Resolut. Chromatogr. 23 (2000) 19.
[8] B.E. Slentz, N.A. Penner, E. Lugowska, F. Regnier, Electrophoresis 22 (2001) 3736.
[9] J. De Smet, P. Gzil, N. Vervoort, H. Verelst, G.V. Baron, G. Desmet, Anal. Chem. 76 (2004) 3716.
[10] J.P. Kütter, O. Gustafsson, R.P.H. Nikolajsen, K.B. Mogensen, Presented at the 28th International Symposium and Exhibit on High Performance Liquid Phase Separations and Related Techniques, Philadelphia, 2004.
[11] P. Gzil, N. Vervoort, G.V. Baron, G. Desmet, Anal. Chem. 75 (2003) 6244.
[12] P. Gzil, G.V. Baron, G. Desmet, J. Chromatogr. A 991 (2003) 169.
[13] P. Gzil, J. De Smet, N. Vervoort, H. Verelst, G.V. Baron, G. Desmet, J. Chromatogr. A 1030 (2004) 53.
[14] B.E. Slentz, N.A. Penner, F. Regnier, J. Sep. Sci. 25 (2002) 1011.
[15] J.H. Knox, J. Chromatogr. Sci. 18 (1980) 453.
[16] P.A. Bristow, J.H. Knox, Chromatographia 10 (1977) 279.
[17] J.C. Giddings, Dynamics of Chromatography, Part I, Marcel Dekker, New York, 1965.
[18] D.K. Schisla, H. Ding, P.W. Carr, E.L. Cussler, AIChE J. 39 (1993) 946.

[19] R. Aris, Proc. R. Soc. A 252 (1959) 538.
[20] J.C. Giddings, J. Chromatogr. 5 (1961) 46.
[21] H. Schlichting, Boundary-Layer Theory, McGraw-Hill, London, 1958.
[22] N. Vervoort, P. Gzil, G.V. Baron, G. Desmet, Anal. Chem. 75 (2003) 843.
[23] N. Tanaka, H. Kobayashi, N. Ishizuka, H. Minakuchi, K. Nakanishi, K. Hosoya, T. Ikegami, J. Chromatogr. A 965 (2002) 35.
[24] H. Poppe, J. Chromatogr. A 778 (1997) 3.
[25] J.H. Knox, J.F. Parcher, Anal. Chem. 41 (1969) 1599.
[26] U. Tallarek, E. Bayer, G. Guiochon, J. Am. Chem. Soc. 120 (1998) 1494.